

Mechanisms of detachment in fibrillar adhesive systems



Pranav Sudersan, Hans-Jürgen Butt, and Michael Kappl*

Max Planck Institute for Polymer Research, Ackermannweg 10, 55128 Mainz, Germany

E-mail: kappl@mpip-mainz.mpg.de

Abstract



Several creatures can climb on surfaces with the help of hairy adhesive pads on their legs. The hairy pad's design allows the animal to rapidly switch between strong adhesion during attachment and weak adhesion during detachment. Previous studies explain this mechanism based on the asymmetric geometry of the hairs, which imparts direction-dependent adhesive properties. However, some insects such as male ladybug beetles are capable of quick detachment despite mostly possessing symmetric "mush-room" shaped hairs. In this study, we theoretically analysed the possible mechanisms by which such a hairy pad can be detached, using a ~~classical~~ spring-based model. We ~~showed~~ that the adhesion force ~~was~~ significantly reduced due to elastic forces when the hairs deform non-uniformly, an effect that we call "*elastic ~~cripling~~*".  Higher number of hairs was shown to further enhance this effect.  Our proposed model illustrates the design advantage provided by hairy adhesive systems, which not only provides strong adhesion, but also allows it to be controlled, making it suitable as organs for fast locomotion. The presented approaches can be potentially used to achieve reversible adhesion in bio-inspired artificial systems without the need of asymmetric structures.

1 Introduction

Over the past few decades, there has been numerous studies to understand how animals such as geckos and insects are able to walk on surfaces ~~in any direction~~ defying gravity. A microscopic observation reveals that, in many cases, animals have a dense array of hairy structures at the end of their legs^{1,2}. These hairy adhesive pads help the animal to stay attached to any surface, supporting its weight, and detach easily at will. Previous attempts to theoretically explain adhesion in hairy pads^{3,4} has followed two fundamental approaches: either by energy balance, or by force balance.

In the energy balance approach, adhesion is characterized by “work of adhesion” (W_{adh}) which is the energy required to separate a pad from the surface. During detachment, the elastic energy stored in the hair is dissipated, which increases W_{adh} and thus adhesion is enhanced^{5,6}. Detachment of an individual hair can be explained based on Kendall’s peeling theory⁷, which predicts low forces at high peeling angles.

In the force balance approach, adhesion is characterized by pull-off force, F_p (or stress, σ_p), which is the minimum force necessary to separate two surfaces from contact. Based on a “cohesive zone model”, Hui et. al.⁸ had identified two regimes of hair detachment: 1) a flaw sensitive regime, where contact failure occurs due to crack propagation leading to low σ_p , 2) a flaw insensitive regime, where the contact interface fails simultaneously, leading to high σ_p . Tian et. al.⁹ had shown that the spatula shaped hair tips in a gecko’s toe allows it to change adhesion by three orders of magnitude by laterally sliding and controlling the pulling angle. Federle¹⁰ had further argued that the curved shape of hairs helps the pad to stay attached when pulled proximally, and easily detached by elastic recoil when pushed distally.

The theories presented so far suggests that low detachment force of a hairy pad can be attained by 1) increasing the stress concentration by peeling the pad at high angles, or 2) laterally shearing the pad before pull-off, which requires the hairs to have an asymmetric geometry. However, some insects like male dock beetles predominantly have nearly symmetric

flat “mushroom” tipped hairs on their pads¹¹. These hairs have been shown to possess superior adhesive strength¹², but the lack of asymmetry in their geometry raises the question of how the beetle can easily detach them during locomotion. Further, fabrication of synthetic mimics with asymmetric micro-pillar structures are generally difficult. It is thus desired to have alternate strategies to achieve reversible adhesion suited for practical applications.

In this work, we theoretically investigate the possible mechanisms of detachment of hairy adhesive pads via the “spring contact model”¹³. This model is based on the force-balance approach, which assumes the pad to behave like an array of springs. We hope our work to provide strategies to control the adhesion force of an artificial micro-pillar adhesive, which has applications in bio-inspired robotic systems.

2 Model

The hairy pad is assumed to be a one dimensional array of N_t hairs, each behaving like a spring with spring constant, k_h , and natural length, $l_{h,0}$ (Figure 1). The array is attached to a linearly deformable leg, assumed to be another spring with spring constant, k_l , and natural length, $l_{l,0}$. The leg is hinged to the array at a distance, s , from the tip along the array. The hinge is at a vertical distance, d_s , from the surface. The hairs are spaced apart by a width, w , and the array is of length, $L = (N_t - 1)w$. The pad is oriented at an angle, θ , while making contact with a flat smooth surface. Each hair can attain a maximum length, $l_{h,p}$, before pull-off, such that its pull-off force, $f_p = k_h(l_{h,p} - l_{h,0})$. F_{net} is the net force on the pad and M_{net} is the the net torque about the hinge, at a particular instant during the detachment process.

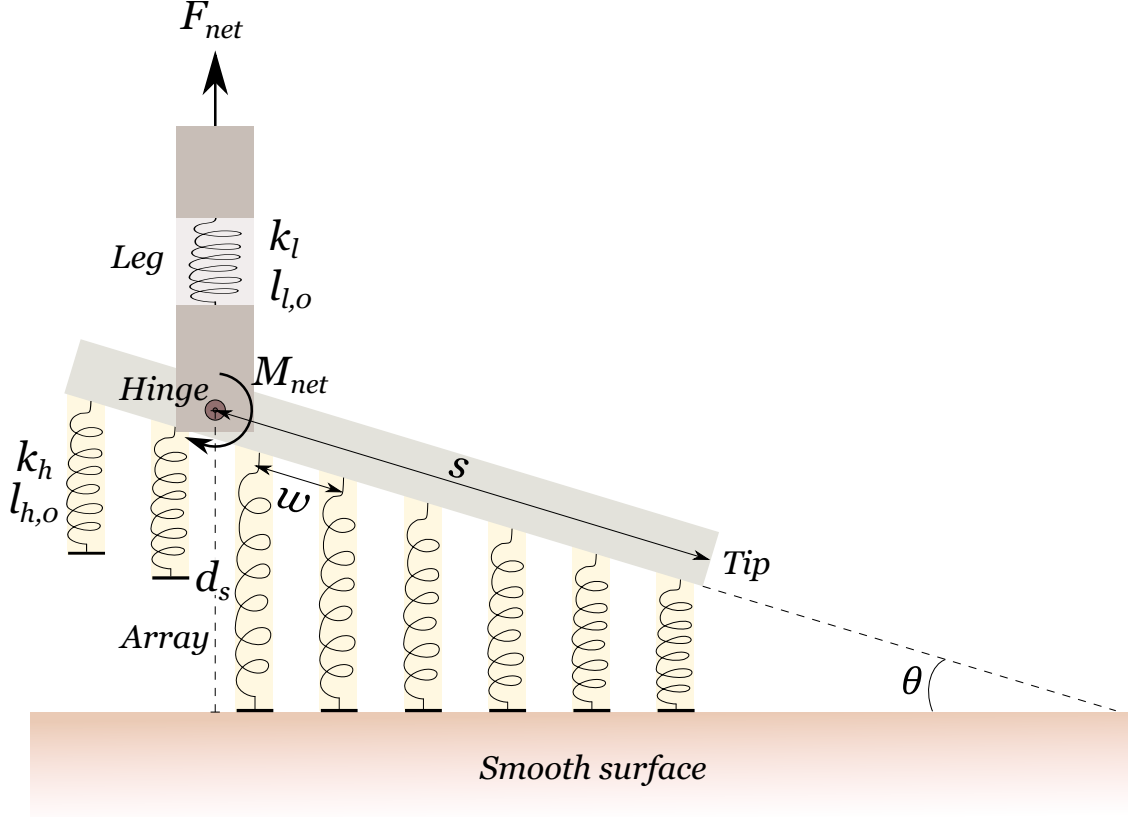


Figure 1: Spring contact model of a hairy adhesive pad. The pad consists of an array of N_t hairs connected to a deformable leg at the hinge. At a particular distance, d_s , n number of hairs are in contact and the array is oriented at a tilt angle, θ , with the surface.

Suppose at a particular instant, there are n hairs in contact with the surface. The net force on the whole pad will be,

$$F_{net} = \sum_{i=1}^n k_h (l_{h,i} - l_{h,0})$$

Simplifying, we get (see Appendix section for derivation):

$$F_{net} = nk_h [d_s - l_{h,0} - \Psi \sin \theta] \quad (1)$$

where, $\Psi = s - \frac{n-1}{2}w$. For a particular value of n , equation 1 is valid until a certain distance, $d_{s,max}$, above which its left most hair will detach. Just before detachment, this hair

will be at its maximum length, $l_{h,p}$. From simple geometry we can thus find:

$$d_{s,max} = l_{h,0} + \frac{f_p}{k_h} + [s - (n - 1)w] \sin \theta \quad (2)$$

Equation 1 will be valid for $d_s \leq d_{s,max}$.

The maximum possible adhesion of the array would be the case when all hairs detach simultaneously:

$$F_{max} = N_t f_p \quad (3)$$

The net torque, M_{net} , about the hinge can be similarly derived (see Appendix):

$$M_{net} = nk_h \cos \theta \left[(d_s - l_{h,0}) \Psi - \left\{ \Psi^2 + \frac{n^2 - 1}{12} w^2 \right\} \sin \theta \right] \quad (4)$$

Let us now consider the scenario where ~~even the leg behind the array deforms~~ together with the hairs. When a hair detaches from the surface, the leg undergoes an elastic recoil due to the stored elastic energy. Suppose the leg relaxes upward by a recoil length, Δl . For n hairs in contact, the force balance before and after a hair detaches is given respectively by:

$$\begin{aligned} \sum_{i=1}^n k_h (l_{h,i} - l_{h,0}) &= k_l (l_l - l_{l,0}) \\ \sum_{i=1}^{n-1} k_h (l_{h,i} + \Delta l - l_{h,0}) &= k_l (l_l - \Delta l - l_{l,0}) \end{aligned}$$

Solving the above two equations for Δl , we get:

$$\Delta l = \frac{f_p}{k_h (n - 1) + k_l} \quad (5)$$

Thus, d_s shifts by Δl in equations 1 and 4 at each event of hair detachment (i.e. when $d_s = d_{s,max}$).

We express the forces and distances in non-dimensional forms, as below:

$$\hat{f}_p = \frac{f_p}{k_h w}, \quad \hat{F}_{net} = \frac{F_{net}}{k_h w}, \quad \hat{d}_s = \frac{d_s - l_{h,0}}{w}, \quad \hat{s} = \frac{s}{w}$$

Here, \hat{f}_p is a parameter which encapsulates the hair's adhesion force, stiffness and array density. Unless specified, positive force values represent attraction by convention.

3 Detachment mechanisms

We consider three possible mechanisms to detach the hairy adhesive pad from a surface: 1) *Fixed pull*, where the pad is pulled vertically up while keeping a fixed hinge, 2) *Free pull*, where the pad is pulled vertically up while keeping the hinge free to allow rotation of the array and 3) *Flex*, where the pad is hinged to an external point and detached in a rotary fashion. To analyse each case in detail, let us assume a pad with $N_t = 25$ hairs and $\hat{f}_p = 0.1$ attached to a stiff leg ($k_l \rightarrow \infty$). The situation of a soft leg ($k_l/k_h = 10$) is also considered for the first two cases involving vertical detachment.

3.1 Fixed pull

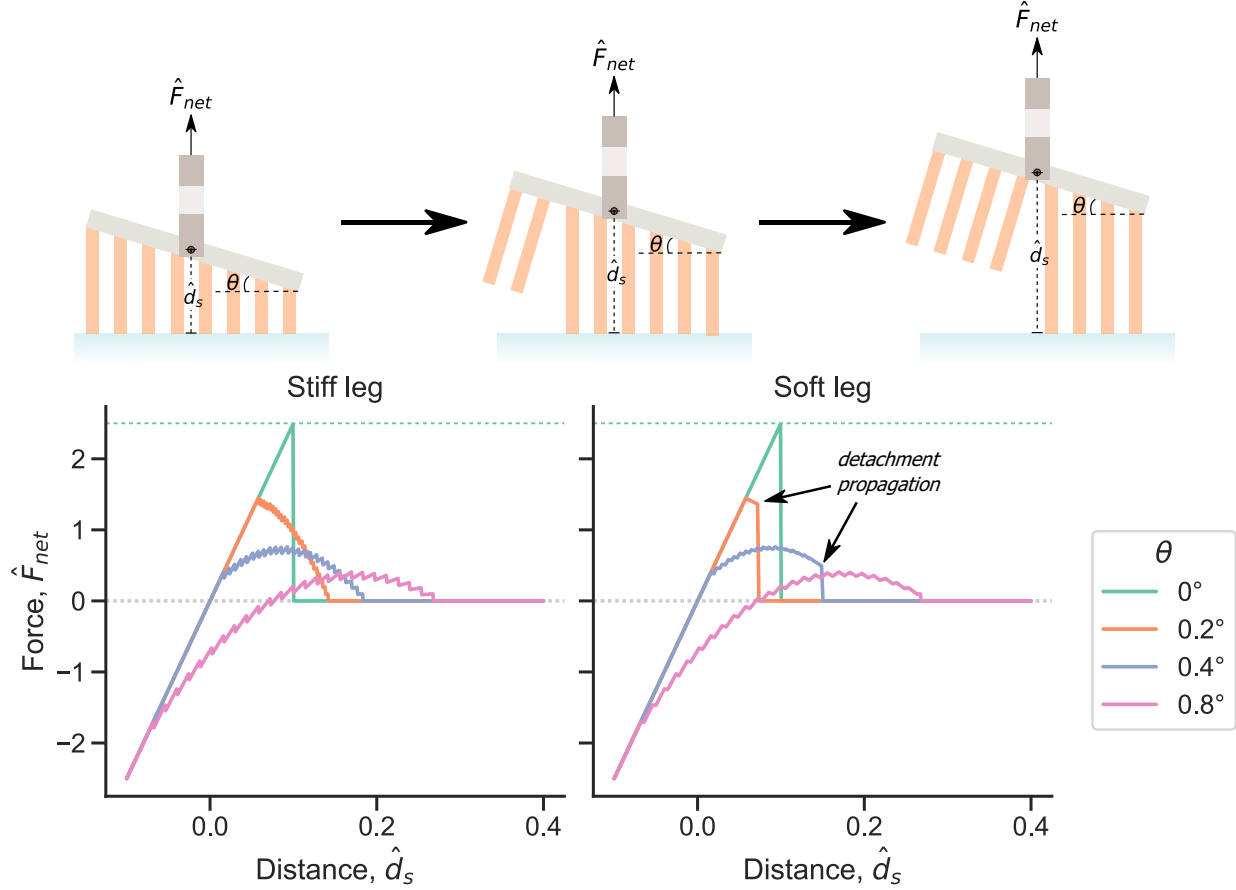


Figure 2: Force distance curves for a hairy pad, pulled vertically upwards with a fixed hinge between the pad and the leg (*Fixed pull*). The tilt angle, θ , of the array is kept fixed during detachment. The leg is either stiff ($k_l \rightarrow \infty$) or soft ($k_l/k_h = 10$). Positive force values represent attraction. The green dashed line represents the maximum possible adhesion for the pad. All values are normalized to dimensionless forms, as described in text.

The hairy adhesive pad can be detached by pulling it vertically upwards while maintaining a constant tilt angle, θ , with the surface. This can be achieved if the hinge connecting the leg to the array is kept fixed. Equations 1, 2 and 3 can be used to get the resulting force-distance curves.

Increasing the tilt of the pad decreases its maximum force or adhesion (Figure 2). Tilting the pad causes an inhomogeneous deformation of hairs, where, on one end they are stretched, while, on the other end they are compressed. The balance of the respective attractive and

repulsive elastic forces of the hairs ultimately results in a decrease in the net force. We term this effect due to non-uniform hair deformation as “*elastic crippling*”. When there is no tilt ($\theta = 0^\circ$), all the hairs undergo identical deformation and ultimately detaches simultaneously after a distance, $\hat{d}_s = 0.1$. Here, no *elastic crippling* occurs and the pad shows the maximum possible adhesion.

For the case of a stiff leg, we see that at small distances, all hairs of the pad are in contact with the surface, resulting in a linear force response. On further pulling, the hairs will start to detach sequentially from left to right, indicated by a characteristic “saw-tooth” fluctuations in the force curves. The hairs of the pad with a higher tilt angle will start to detach first, followed by the ones with a lower tilt.

For the case of a soft leg, we observe a similar effect of tilt angle on the force curves as before. The maximum adhesion force at a particular tilt is the same as that for the stiff leg. The “saw-tooth” fluctuations are however minimized due to the leg’s deformation, leading to a “dampened” force response. Interestingly, the force abruptly drops to zero for the angles 0.2° and 0.4° . This is an effect of the elastic recoil of the leg while each hair loses contact during the detachment process (equation 5). The length difference between the detached hair just before it breaks contact and its adjacent hair is $w \sin \theta$. If the leg’s recoil length, $\Delta l > w \sin \theta$, the adjacent hair will be stretched more than its maximum length ($l_{h,p}$), and thus will also detach, leading to further recoil of the leg. Equation 5 shows that Δl increases with every subsequent loss of hair contact if θ is kept constant. This implies that, once initiated, the leg’s recoil will always be large enough to detach every remaining hair, resulting in a spontaneous propagation of the detachment front until the pad completely breaks contact with the surface.

3.2 Free pull

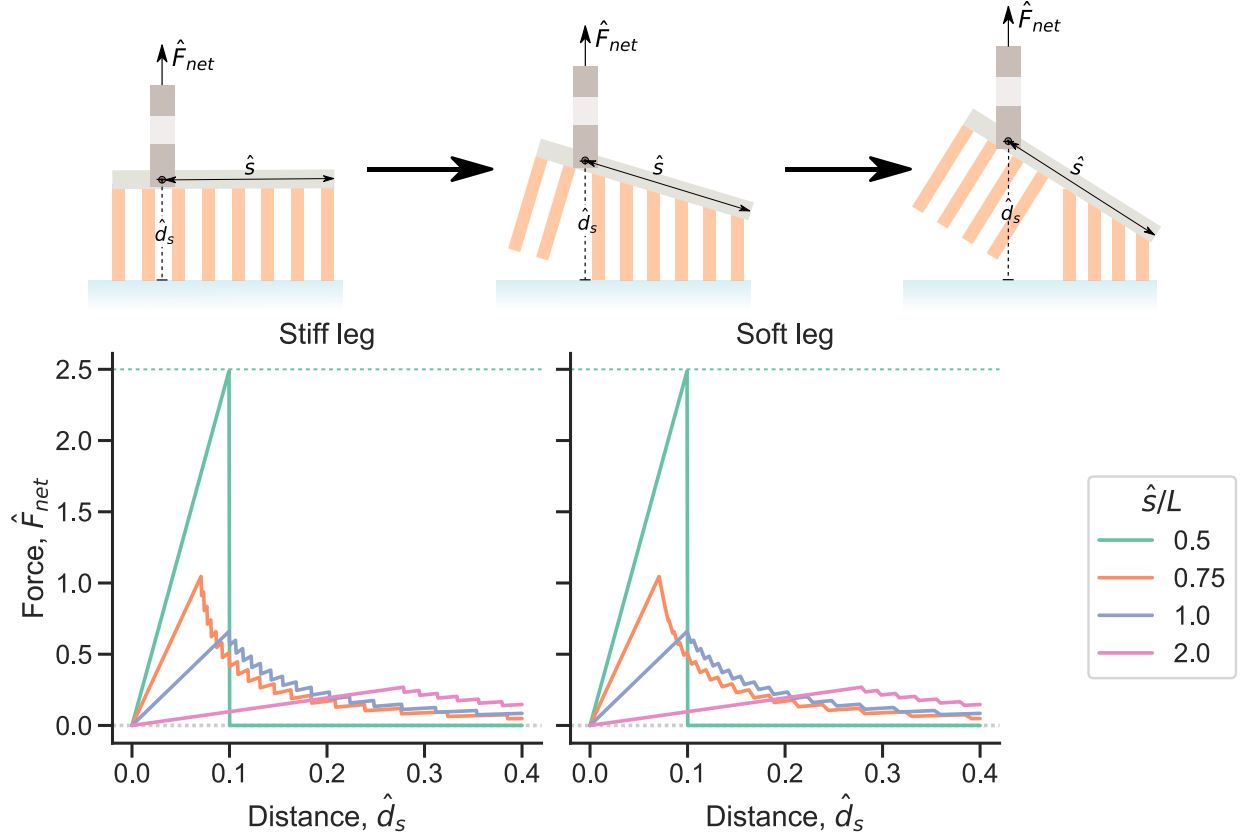


Figure 3: Force distance curves for a hairy pad, pulled vertically upwards with a free hinge between the pad and the leg (*Free pull*). The leg is either stiff ($k_l \rightarrow \infty$) or soft ($k_l/k_h = 10$). Positive force values represent attraction. The green dashed line represents the maximum possible adhesion for the pad. All values are normalized to dimensionless forms, as described in text.

Similar to the previous case, we once again consider the situation where the adhesive pad is pulled vertically upwards for detachment. However now, the leg is assumed to be hinged freely to the array. In this case, the array will reorient itself such that the net torque about the hinge remains zero during the entire detachment process. At any given instant, the tilt angle, θ , can be found by setting M_{net} to zero in equation 4 to get:

$$\theta(\hat{d}_s, n) = \arcsin \left[\frac{\left(\hat{s} - \frac{n-1}{2}\right) \hat{d}_s}{\left(\hat{s} - \frac{n-1}{2}\right)^2 + \frac{n^2-1}{12}} \right] \quad (6)$$

Using the above relation together with equations 1, 2 and 3, we can find force-distance curves during a free vertical pull of the adhesive pad. Since the position of the hinge will influence the net torque, we use the ratio, \hat{s}/L , to study its effect on the detachment forces.

Maximum adhesion is seen when the hinge is positioned at the centre of the array, i.e. $\hat{s}/L = 0.5$ (Figure 3). Here, the net torque due to the hairs is balanced by symmetry and the array remains parallel to the substrate until all hairs detach simultaneously at $\hat{d}_s = 0.1$. Shifting the position of the hinge further away from the array centre leads to lower forces or adhesion. The resulting torque imbalance will tilt the array, which reduces the net force due to the *elastic crippling* effect. Higher \hat{s}/L increases the net torque to be balanced, leading to a higher tilt of the array and thus lower net force.

The force curves look qualitatively different compared to the previous case of *fixed pull*. A sharp maxima is seen, coinciding with the point when the first hair detaches. Beyond this, the force starts to decrease sharply and once again shows the characteristic “saw-tooth” fluctuations as the subsequent hairs detach in sequence. Nearly identical trend is seen for both a stiff and a soft leg. The elastic recoil of the leg does slightly reduce the amplitude of the fluctuations for the soft leg case. However, no abrupt drop in the force is seen like before. As the hairs detach, the array gets tilted more and more, making it less likely for the recoil length, Δl , to exceed $w \sin \theta$ and detach the next hair. Thus here, we don’t see any propagation of the detachment front when the leg is soft.

3.3 Flex

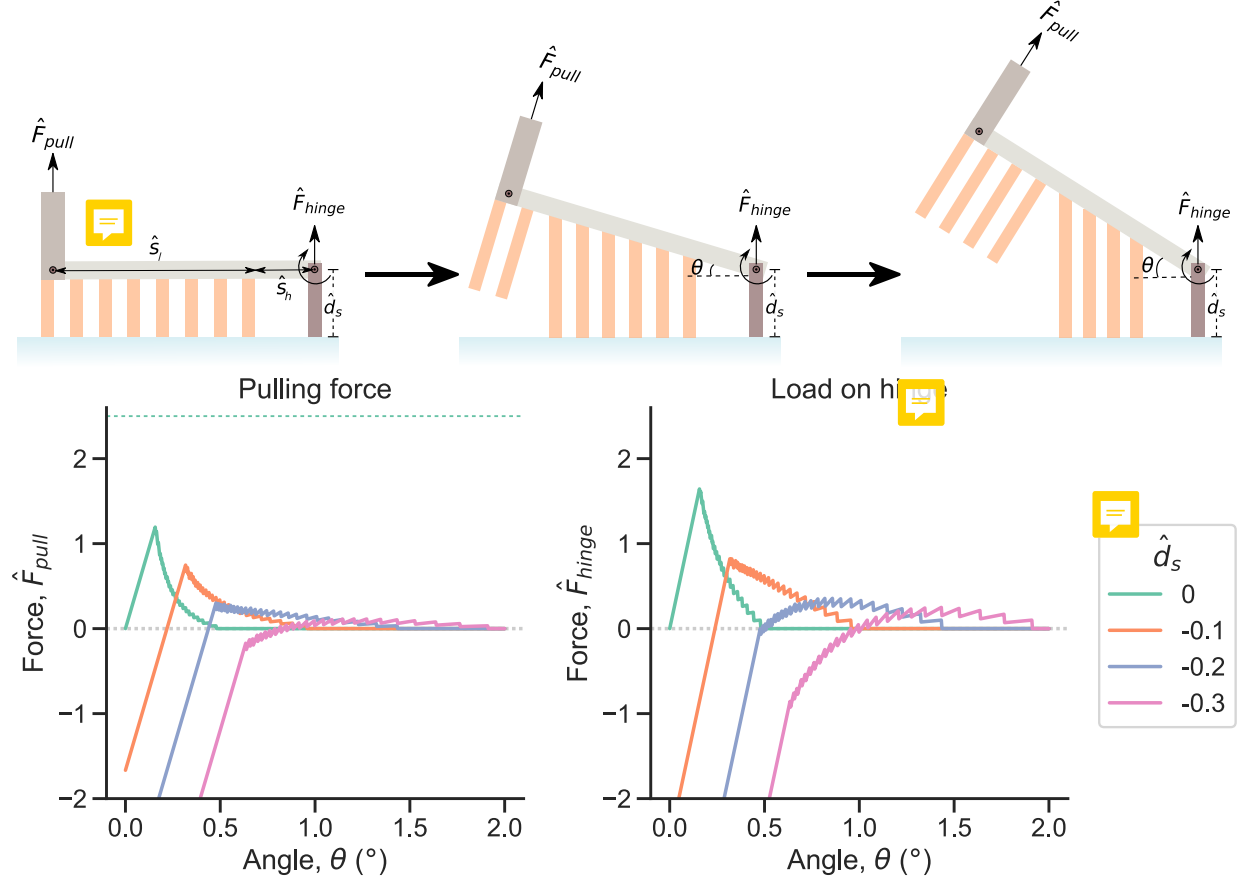


Figure 4: Force curves for a hairy pad detached by flexing it about an external hinge point. \hat{F}_{pull} is the pulling force necessary to apply the torque about the hinge for detachment. \hat{F}_{hinge} is the normal reaction force on the hinge. Here, $s_l/L = 1$ and $s_h/w = 10$. The green dashed line represents the maximum possible adhesion for the pad. All values are normalized to dimensionless forms, as described in text.

Instead of a vertical pull, the adhesive pad can also be detached by flexing it about a hinge located outside the array. Such a mode of detachment will be driven by a torque applied by the leg to rotate the pad around the hinge until all the hairs lose contact. Let s_h be the position of the hinge to the right of the array tip and s_l be the position of the leg to the left of the array tip. At any particular instant, the pulling force applied by the leg, $F_{pull} = M_{net} / (s_l + s_h)$, where M_{net} is given by equation 4 for $s = -s_h$. Equation 1 will give us the load acting on the hinge, F_{hinge} , to support the applied torque. Let us keep the lateral

position of the leg and the hinge fixed, such that, $s_l/L = 1$ and $s_h/w = 10$ and vary the vertical hinge distance, d_s .

Decreasing the hinge distance reduces the pulling force necessary to undergo detachment by flexing (Figure 4). One can imagine that initially, when the array is parallel to the surface, a lower value of d_s means the hairs are at a more compressed state. On flexing the pad around the hinge, the tilted array will once again lead to an *elastic crippling* effect due to the inhomogeneous deformation of hairs, which is enhanced for smaller \hat{d}_s . This results in a decrease in the net torque and thus lower \hat{F}_{pull} . \hat{F}_{pull} can be further reduced of course by increasing the lever arm (\hat{s}_l).

Detachment by flexing requires that the point of hinge remains fixed and stable during the process. We see that generally, the normal load, acting on the hinge, \hat{F}_{hinge} , follows a similar trend as \hat{F}_{pull} . For low values of \hat{d}_s , \hat{F}_{hinge} goes to negative values as a reaction to the compressed hairs. Thus, the hinge should adhere well with the surface to resist the negative load in such cases. As the detachment progresses, the array exerts a positive load on the hinge, essentially transferring the array's normal adhesion onto the hinge as load.

4 Discussion

In order to characterize how a particular detachment mechanism influences the adhesion of the pad, we introduce a parameter, *reduction factor*, defined as:

$$r = \frac{N_t f_p}{F_{adh}} \quad (7)$$

Here, F_{adh} is the adhesion force required to detach the pad from the surface following a given mechanism and $N_t f_p$ is the maximum possible adhesion of the pad (equation 3). Reduction factor, r , represents the extent to which the adhesion can be reduced by manipulating the mode of detachment. A large value of r implies that adhesion can be reduced by a higher factor, and thus is more suitable to easily detach.

Effect of \hat{f}_p : The dimensionless parameter, $\hat{f}_p = \frac{f_p}{k_h w}$, governs the strength and compliance of the array, where, high values represent a dense array of strong and soft hairs. Let us consider the case of an adhesive pad with $N_t = 25$ hairs and look at how \hat{f}_p influences the reduction factor in each mode of detachment (Figure 5). From the heat maps, one can generally say that lower values of \hat{f}_p increases the reduction factor and thus provides a greater possibility of controlling adhesion.

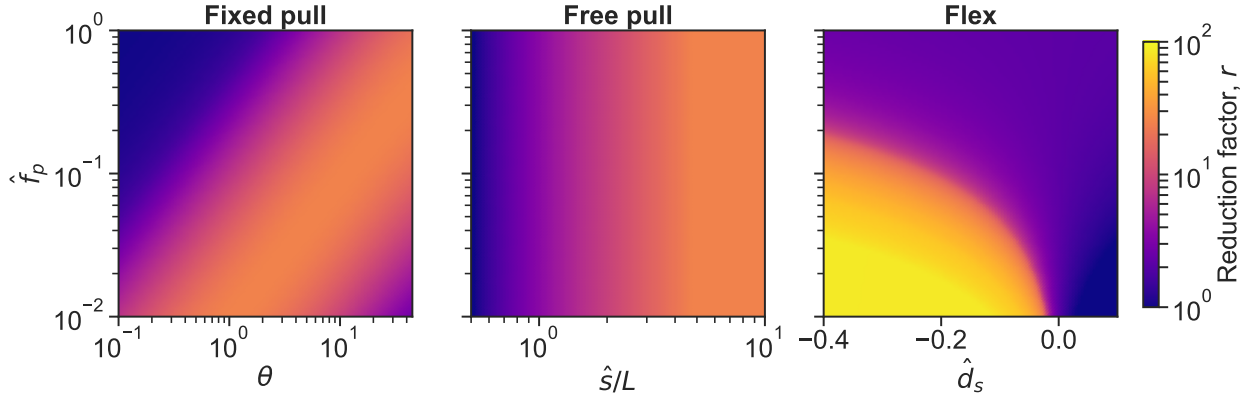


Figure 5: Heat maps showing the effect of the dimensionless parameter, $\hat{f}_p N_t$, on the reduction factor for each mode of detachment. Here, the number of hairs, $N_t = 25$. All values are normalized to dimensionless forms, as described in text.

When detachment follows the *fixed pull* method, for a constant \hat{f}_p , the reduction factor increases with increasing tilt angle, θ , and then decreases, showing a maximum of 25 at an intermediate θ . Higher values of \hat{f}_p shifts this maximum point to higher values of θ . This trend relates to the *elastic crippling* effect discussed before. Smaller value of θ brings a proportion of hairs under compression, reducing the adhesion and thus increasing r . On further tilting the array, eventually the proportion of stretched hairs overcomes the one under compression, which ultimately reduces r at high θ . When the individual hairs show strong adhesion (i.e. for high \hat{f}_p), a greater tilt is necessary to bring the net adhesion of the array down.

For the case of detachment via *free pull*, \hat{f}_p has no influence on the reduction factor. On the other hand, shifting the position of the hinge further away from the array (i.e. high \hat{s}/L)

results in large values of r . In this scenario, the higher torque exerted by the array leads to a higher tilt, and thus increases the reduction factor via *elastic crippling*, saturating to the maximum value of 25.

For detachment by *flexing*, the reduction factor increases for higher initial compression of hairs (low \hat{d}_s). The pad notably shows a much higher reduction factor at low values of \hat{f}_p and \hat{d}_s , with values as high as 100. Since this mode of detachment is driven by torque, the pulling force necessary to provide the torque can be decreased without any limit simply by having a long lever arm (\hat{s}_l). In contrast, for the previous cases of *free pull* and *fixed pull*, the reduction factor is capped to the maximum number of hairs in the array ($N_t = 25$). Here, *elastic crippling* can only reduce the array's adhesion force from N_t hairs down to a single hair.

Effect of N_t : Let us now fix $\hat{f}_p = 0.1$ and investigate the influence of the number of hairs, N_t , on the reduction factor (Figure 6). The heat maps show that high N_t increases r irrespective of the mode of detachment. Under a tilted state, more number of hairs are compressed when N_t is high, which reduces the net adhesion. This highlights the advantage of having a split contact design found in many biological systems. Higher number of hairs offer a better control over adhesion and thus is more suited for reversible attachment and detachment during locomotion. The specific trends of reduction factor for each mode of detachment can be understood by similar arguments of *elastic crippling*, as discussed in the previous section.

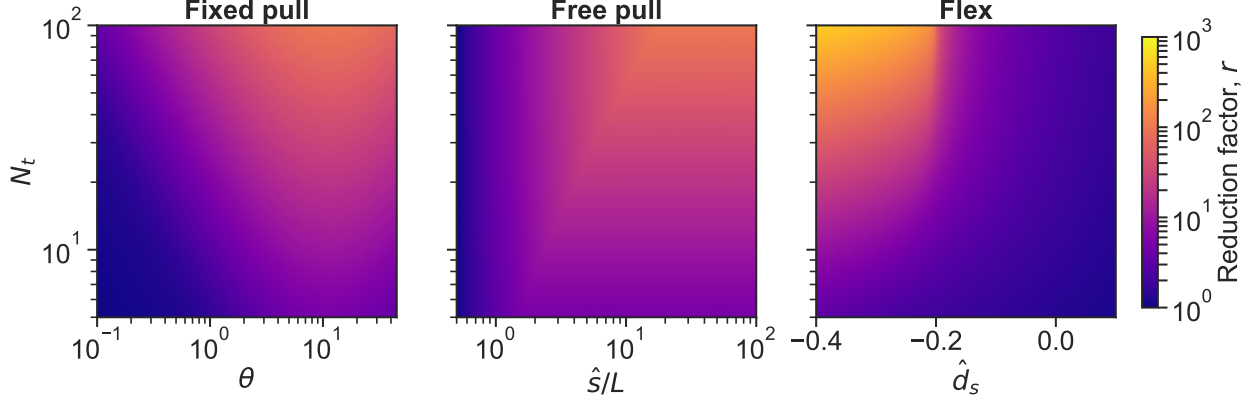


Figure 6: Heat maps showing the effect of the number of hairs, N_t , on the reduction factor for each mode of detachment. Here, the dimensionless parameter, $\hat{f}_p = 0.1$. All values are normalized to dimensionless forms, as described in text.

Detachment pathways: Based on the three modes of detachment discussed in the previous section, one can think of several strategies to detach a hairy adhesive pad from the surface. To illustrate this, let us consider the adhesive system of a dock beetle. The beetle is known to have 3 sets of hairy adhesive pads in each of their legs, each possessing hairs of different geometries. To keep our analysis simple, we will assume it to have only two pads, ignoring the tiny centre pad. The distal and proximal pads possess roughly 500 and 1000 hairs, respectively¹¹. Assuming the pads to be rectangular arrays of 20×25 and 40×25 hairs, we can model this as a one-dimensional system of 20 and 40 hairs, respectively, by combining the hairs along the width. Based on reported measurements¹⁴, the beetle’s combined “hair” is thus considered to have an effective pull-off force, $f_p = 0.5 \times 25 = 12.5 \mu\text{N}$ and spring constant, $k_h = 0.5 \times 25 = 12.5 \text{ N/m}$. The beetle’s hairs are approximately $l_{h,0} = 40 \mu\text{m}$ long, spaced $w = 10 \mu\text{m}$ apart. The adhesive pad also has a claw, around $200 \mu\text{m}$ long, and the leg is connected roughly at the end of the proximal pad. This will put $\hat{s}_h = 20$ and $s_l/L = 1$, measured relative to the tip of the distal pad. The beetle’s leg is assumed to possess two joints which could serve as a hinges for rotation (H_1 and H_2 in Figure 7 inset). The claw can be used as an external hinge (H_3) by flexing the pad around it.

Based on the above assumptions, we can come up with force-distance curves to detach

the beetle's leg via various pathways (Figure 7). First, let us assume the hinge H_2 to be fixed, such that both the distal and proximal pads can be combined into be a single long pad with $N_t = 60$ hairs. Path 1 shows the case where the pad shows maximum possible adhesion. Here, the pad is vertically pulled upwards while keeping the array perfectly parallel to the surface. If the pad is detached by keeping H_1 fixed and maintaining a tilt of 1° with the surface (path 2), the forces dramatically reduces, with around 10 times reduction in the adhesion compared to path 1. We can also detach the pad by switching between the different mechanisms. Path 3 shows one such example, where, initially the leg is pulled vertically up while keeping H_1 fixed, stretching the hairs. On reaching point a , H_1 is set free, which results in a sudden drop in force due to the excess torque by the stretched hairs, tilting the array. Beyond this, the force curve follows the free pull mechanism, with ~ 3.5 times reduction in adhesion. An alternate strategy of switching between mechanisms would be to first apply a load on the pad (path 4) and compress the hairs until point b . Beyond this point, the claw can be used as a hinge to detach the pad via flexing it around H_3 , which once again reduces the adhesion force. Now, if we assume the hinge H_2 to be free such that two pads can react distinctly, we can consider the scenario where the proximal pad is flexed around the distal pad at H_2 while keeping H_1 fixed (path 5). After the proximal pad has completely detached, H_1 can be freed up at point c to detach the distal pad via *free pull* with very little force. This pathway results in a ~ 5 times reduction in adhesion.

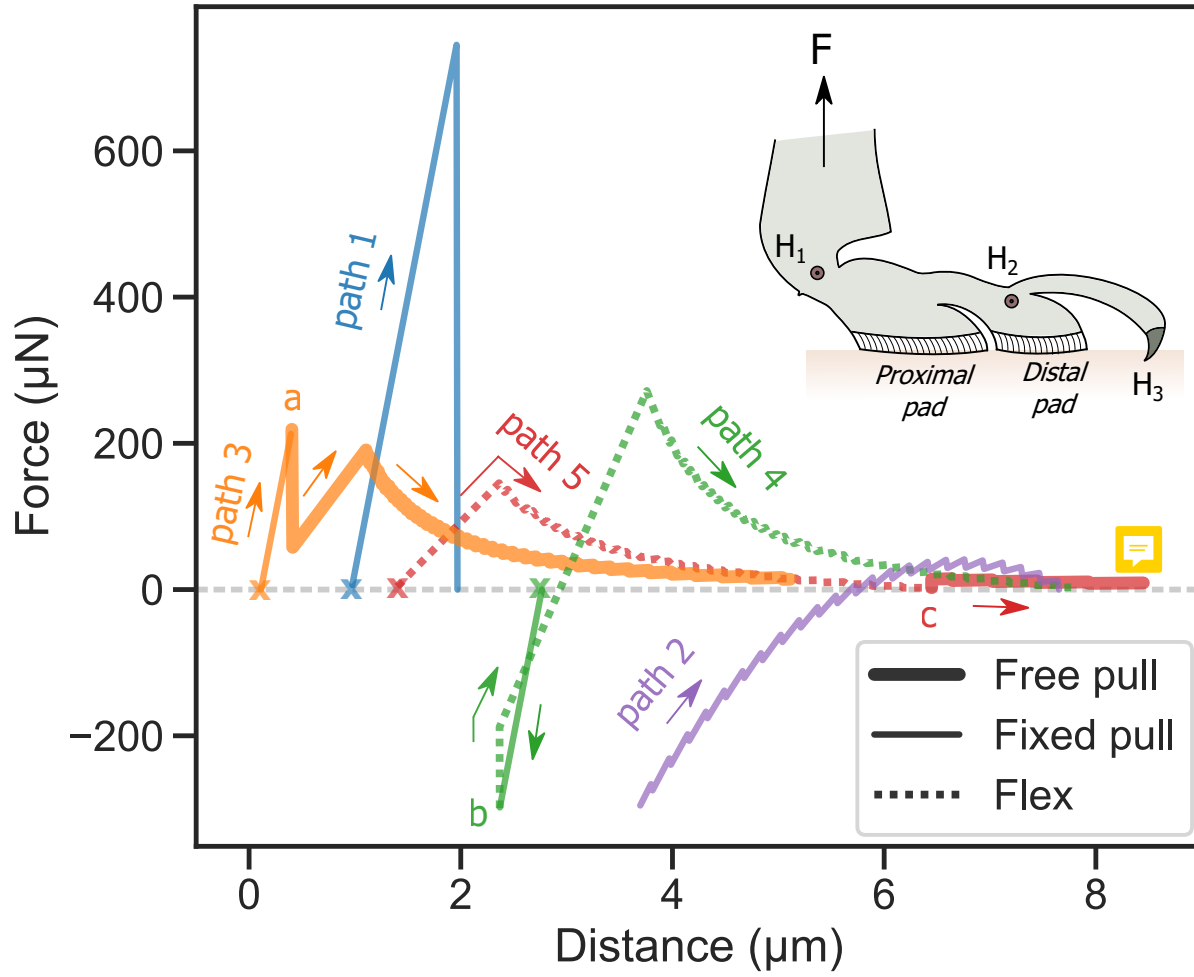


Figure 7: Force distance curves showing possible detachment pathways for a dock beetle's leg, derived from the spring contact model. The curves are shifted laterally for clarity. Colours represent the distinct detachment pathways, as labelled correspondingly, with arrows indicating the direction of retraction. Legend shows the specific detachment mechanism followed by a region of the pathway. The inset schematic shows the location of different hinges (H_1 , H_2 and H_3) employed by the leg.


The above analysis illustrates how the design of the beetle's hairy adhesive pads is suitable for modulating its adhesion. Effective control and release of its leg joints can help the insect to reduce the pad's adhesion, allowing it to detach easily with little effort. High reduction in adhesion is seen when the pad is tilted relative to the surface during detachment, as a result of *elastic crippling*. As far as our knowledge, there is no direct experimental evidence that beetles can modulate its adhesion by taking advantage of this effect. Considering that

hair deformation occurs at length scales below 10 μm , direct observation of this effect on running beetles would be challenging. A recent study on PDMS micro-pillar arrays, however, does indeed show a strong reduction in the adhesion force due to slight misalignments with the surface¹⁵. Based on previously reported microscopic investigation of freely walking dock beetles¹⁶, we argue that the following experimental observations provide support to our proposed theory: 1) The detachment was shown to follow a three-dimensional twist of the leg, which suggests a complex inhomogeneous deformation of hairs across the array, leading to *elastic crippling*. 2) The beetle can at times instantaneously detach all its legs and “drop” itself while upside down. This could be explained by the beetle freeing up its leg joints and using just its body weight to provide the necessary force to detach all its legs via *free pull* (similar to path 3 above). 3) Only a fraction of the beetle’s pads made contact with the surface during locomotion, which indicates that the pads should be in a slightly tilted state. This not only reduces the contact area, but also non-uniformly deforms the hairs, both leading to a reduction in adhesion for easy detachment. 4) Contact images showed that the array “peels” from the proximal to distal direction during detachment. However, the beetle’s hairs are attached to a relatively stiff backing¹⁷, so it wouldn’t be able to “peel” its array, since peeling, strictly speaking, depends on the elastic contribution of a thin flexible backing as it bends during the process⁷. Rather, the “peeling” observed in the beetle’s case should be a result of the pad detaching from the surface in a tilted orientation, causing the hairs to detach in sequence. 5) The time scale of detachment was reported to be an order of magnitude shorter than the attachment time scale, which could be a result of the elastic recoil of the leg causing a spontaneous propagation of the detachment front (Figure 2).

There exists a limit to how much the pad can tilt, depending on its geometry and material properties. Suppose the hair has a maximum linear elastic strain limit, ε_m , and natural length, $l_{h,0}$. Based on Figure 1, if the right most hair is compressed to its elastic limit, we can show from simple geometry, that, the corresponding maximum limit in tilt angle is given

by:

$$\theta_{limit} = \arctan \frac{l_{h,0} \varepsilon_m}{(N_t - 1) w}$$

θ_{limit} will limit the reduction factor for each of the detachment mechanisms presented. Large deformation of hairs can also lead to buckling, which will further limit the reduction in adhesion due to the smaller effective modulus. Thus, the geometry of the individual hairs is also crucial in effectively reducing adhesion by *elastic crippling*. Ideally, long hairs with large diameters would be preferable to eliminate buckling while at the same time providing a large range of angles to which the pad can be tilted. 

5 Conclusion

Non-homogenous deformation of hairs results in significant reductions in the adhesion of a hairy pad system. Such a condition can be achieved by either 1) pulling the pad while maintaining a constant tilt angle, 2) pulling the pad while maintaining a free leg joint or 3) flexing the pad around an external hinge. Strategic control of the joint's mobility can allow the leg to easily switch between the given mechanisms, thus providing a simple way to reduce adhesion as per necessity. The presence of a deformable leg can further trigger a spontaneous propagation of hair detachment due to the leg's elastic recoil, making it suitable for fast detachment. Arrays with low \hat{f}_p and large number of hairs, with a hair geometry that allows for large deformations while avoiding buckling represent the optimal design conditions to maximize the range of control over adhesion. The proposed theory is supported by previously reported experimental observations of leg detachment in dock beetles and opens up new strategies to achieve reversible adhesion in bio-inspired artificial adhesives without the need of asymmetric structures

6 Acknowledgment

We are grateful to Thomas Endlein, Renè Hensel and Bat-El Pinchasik for fruitful discussions. This work was funded by *Deutsche Forschungsgemeinschaft* (Grant number: PI 1351/2-1).

A Appendix

A.1 Derivation

When $\theta > 0^\circ$, the hairs will detach sequentially from left to right. Suppose at a particular instant (Figure 1), there are n hairs in contact with the surface. The origin is assumed to lie at the midpoint along the surface where the n hairs are making contact. The pad is at a vertical distance, d' , from the origin. For a particular tilt angle, θ , the net force on the whole pad at a distance d from the surface is,

$$F_{net}(d, n, \theta) = \sum_{i=1}^n k_h (l_{h,i} - l_{h,0})$$

$l_{h,i}$ is the length of the i^{th} hair, which is at a distance x from the origin. From simple geometry, $l_{h,i} = d' - x \tan \theta$. Substituting in above and noting that $\sum_{i=1}^n x = 0$ by symmetry, we get:

$$F_{net}(d, n, \theta) = nk_h (d' - l_{h,0})$$

From geometry, d and d' is related as:

$$\frac{d}{\tan \theta} - \frac{d'}{\tan \theta} = \frac{(N_t - 1) w \cos \theta}{2} - \frac{(n - 1) w \cos \theta}{2}$$

Eliminating d' from the above two equations, we find the net force on the pad as a

function of distance to be:

$$F_{net}(d, n, \theta) = nk_h \left(d - l_{h,0} - \frac{N_t - n}{2} w \sin \theta \right) \quad (\text{A.1})$$

For a particular value of n , equation A.1 is valid until a certain distance, d_{max} , above which its left most hair will detach. Just before detachment, this hair will be at its maximum length, $l_{h,p}$. Once again from geometry, we see that d_{max} and $l_{h,p}$ is related as:

$$\frac{l_{h,p}}{\tan \theta} - \frac{d_{max}}{\tan \theta} = (n - 1) w \cos \theta - \frac{(N_t - 1) w \cos \theta}{2}$$

Substituting $l_{h,p} = \frac{f_p}{k_h} + l_{h,0}$ in above and simplifying, we get:

$$d_{max}(n, \theta) = l_{h,0} + \frac{f_p}{k_h} + \left(\frac{N_t + 1}{2} - n \right) w \sin \theta \quad (\text{A.2})$$

Equation A.1 is valid for $d \leq d_{max}$. We can substitute d_{max} in equation A.1 to get the force at which the left most hair detaches from the surface:

$$F_{net}(n, \theta) = nf_p - \frac{n(n-1)}{2} k_h w \sin \theta \quad d = d_{max} \quad (\text{A.3})$$

Equation A.3 is the maximum force necessary to detach one hair of the pad when there are n hairs in contact. During this sequential detachment of hairs, there exists a maximum in force at a particular number of contacts, N_{max} . Differentiating equation A.3 and equating it to zero we find:

$$N_{max} = \frac{f_p}{k_h w \sin \theta} + \frac{1}{2} \quad (\text{A.4})$$

Substituting the above in equation A.3, the maximum adhesion force of a pad during a sequential detachment of its N_t hairs will be:

$$F_{adh}(\theta) = \begin{cases} \frac{f_p}{2} \left[\frac{f_p}{k_h w \sin \theta} + 1 \right] + \frac{k_h w \sin \theta}{8} & N_t \geq N_{max} \\ N_t f_p - \frac{N_t(N_t-1)}{2} k_h w \sin \theta & N_t < N_{max} \end{cases} \quad (\text{A.5})$$

References

- (1) Hooke, R. *Micrographia, or, Some physiological descriptions of minute bodies made by magnifying glasses : with observations and inquiries thereupon*; The Royal Society, 1665.
- (2) Stork, N. E. Experimental Analysis of Adhesion of *Chrysolina Polita* (Chrysomelidae: Coleoptera) on a Variety of Surfaces. *The Journal of Experimental Biology* **1980**, *88*, 91.
- (3) Labonte, D.; Federle, W. Scaling and biomechanics of surface attachment in climbing animals. *Philos Trans R Soc Lond B Biol Sci* **2015**, *370*, 20140027.
- (4) O'Rourke, R. D.; Steele, T. W. J.; Taylor, H. K. Bioinspired fibrillar adhesives: a review of analytical models and experimental evidence for adhesion enhancement by surface patterns. *Journal of Adhesion Science and Technology* **2016**, *30*, 362–391.
- (5) Persson, B. N. J. On the mechanism of adhesion in biological systems. *The Journal of Chemical Physics* **2003**, *118*.
- (6) Jagota, A.; Stephen, J. B. Mechanics of Adhesion through a Fibrillar Microstructure. *Integrative and Comparative Biology* **2002**, *42*, 1140–1145.
- (7) Kendall, K. Thin-film peeling-the elastic term. *Journal of Physics D: Applied Physics* **1975**, *8*, 1449–1452.
- (8) Hui, C. Y.; Glassmaker, N. J.; Tang, T.; Jagota, A. Design of biomimetic fibrillar interfaces: 2. Mechanics of enhanced adhesion. *J R Soc Interface* **2004**, *1*, 35–48.

- (9) Tian, Y.; Pesika, N.; Zeng, H.; Rosenberg, K.; Zhao, B.; McGuiggan, P.; Autumn, K.; Israelachvili, J. Adhesion and friction in gecko toe attachment and detachment. *Proceedings of the National Academy of Sciences of the United States of America* **2006**, *103*, 19320–19325.
- (10) Federle, W. Why are so many adhesive pads hairy? *J Exp Biol* **2006**, *209*, 2611–21.
- (11) Bullock, J. M.; Federle, W. Division of labour and sex differences between fibrillar, tarsal adhesive pads in beetles: effective elastic modulus and attachment performance. *J Exp Biol* **2009**, *212*, 1876–88.
- (12) Carbone, G.; Pierro, E.; Gorb, S. N. Origin of the superior adhesive performance of mushroom-shaped microstructured surfaces. *Soft Matter* **2011**, *7*, 5545–5552.
- (13) Schargott, M.; Popov, V. L.; Gorb, S. Spring model of biological attachment pads. *Journal of Theoretical Biology* **2006**, *243*, 48–53.
- (14) Bullock, J. M.; Federle, W. Beetle adhesive hairs differ in stiffness and stickiness: in vivo adhesion measurements on individual setae. *Naturwissenschaften* **2011**, *98*, 381–7.
- (15) Booth, J. A.; Bacca, M.; McMeeking, R. M.; Foster, K. L. Benefit of Backing-Layer Compliance in Fibrillar Adhesive Patches-Resistance to Peel Propagation in the Presence of Interfacial Misalignment. *Advanced Materials Interfaces* **2018**, *5*, 1800272.
- (16) Gernay, S. M.; Labousse, S.; Lambert, P.; Compere, P.; Gilet, T. Multi-scale tarsal adhesion kinematics of freely-walking dock beetles. *J R Soc Interface* **2017**, *14*.
- (17) Peisker, H.; Michels, J.; Gorb, S. N. Evidence for a material gradient in the adhesive tarsal setae of the ladybird beetle *Coccinella septempunctata*. *Nat Commun* **2013**, *4*, 1661.